Nanoscale

PAPER

View Article Online
View Journal | View Issue

Cite this: *Nanoscale*, 2015, **7**, 11971

SnO_2 quantum dots decorated on RGO: a superior sensitive, selective and reproducible performance for a H_2 and LPG sensor†

R. K. Mishra,*[a] S. B. Upadhyay,[b] Ajay Kushwaha,[c] Tae-Hyung Kim,[d] G. Murali,[a] Ranjana Verma,[e] Manish Srivastava,[f] Jay Singh,[g] P. P. Sahay[b] and Seung Hee Lee*[a]

Received 1st May 2015,
Accepted 30th May 2015

DOI: 10.1039/c5nr02837j

www.rsc.org/nanoscale

We report the H_2 and LPG gas sensing behavior of RGO/SnO_2 QDs synthesized by a surfactant assisted hydrothermal method. The RGO/SnO_2 QD based sensor shows a high response of ~89.3% to H_2 and ~92.4% to LPG for 500 ppm test gas concentration at operating temperatures of 200 °C and 250 °C, respectively. Further, the RGO/SnO_2 QD based sensor shows good selectivity for H_2 and LPG in the presence of other interfering gases such as ammonia, chloroform, toluene, benzene, acetone, *n*-butylacetate, acetic acid and formic acid. We observed that the gas response to H_2 is 29.8 times higher than that to acetic acid whereas the gas response to LPG is 17.8 times higher than that to formic acid. Long-term analyses have also been performed to demonstrate the reproducible nature of the RGO/SnO_2 QD based sensor over passing time which shows excellent reproducibility.

Introduction

Solid state gas sensors are well known for their high sensitivity, good selectivity and stability, which in combination with their inexpensive production, simple nature, power efficiency and miniature sizes have made them ubiquitous and extensively used in various applications.[1–4] Recently, a new generation of gas sensors has been reported using graphene and graphene/metal oxide nanocomposites.[5–9] Among metal oxide semiconductors (MOS), tin oxide (SnO_2) is particularly important, as an intrinsic n-type wide band gap (3.6 eV at 300 K) semiconductor[10] and has drawn much attention because of its good optical and electrical properties. It exhibits n-type conductivity due to its interstitial Sn atoms and oxygen vacancies, which act as donors in the host matrix.[11] SnO_2 nanostructures have shown potential applications in various devices *e.g.* field effect transistors,[12] light emitting diodes,[13] dye-sensitized solar cells,[14] supercapacitors,[15] lithium ion batteries[16] and gas sensors.[17]

Graphene, a two dimensional counterpart of three-dimensional graphite, comprises a single layer of carbon atoms and is a rising star on the horizon of nano-materials & technology, solid-state physics, materials science, and nanoelectronic devices.[18] In addition, graphene possesses outstanding physical properties such as quantum electronic transport, extremely high mobility and high surface to volume ratio. Graphene based nanostructure materials have attracted great interest from researchers due to their numerous applications in organic light emitting diodes, solar cells, chemical and biological gas sensors,[19] transistors, photovoltaics, and photosensors. The commonly used methods for the preparation of graphene and reduced graphene oxide (RGO) are micromechanical cleavage of graphite,[20] chemical vapor deposition (CVD),[21] epitaxial growth,[22] using organic precursors,[23] chemical reduction of exfoliated graphene oxide[24] and electrochemical reduction.[25] Since graphene possesses a monoatomic layer structure and excellent electrical properties, it could be a fascinating material for gas sensing application. In principle, charge carriers in an individual graphene sheet delocalize over the entire sheet and can travel thousands of interatomic distances without scattering because of its zero band gap semiconducting nature, very high in-plane conductivities and very high Fermi velocity.[26] However, its poor interactions with

[a]*Applied Materials Institute for BIN Convergence, Department of BIN Fusion Technology and Department of Polymer-Nano Science and Technology, Chonbuk National University, Jeonju, Jeonbuk 561-756, Korea.*
E-mail: rajneeshmishra08@gmail.com, lsh1@chonbuk.ac.kr; Tel: +82-63-270-2343
[b]*Department of Physics, Motilal Nehru National Institute of Technology, Allahabad 211004, India*
[c]*Department of Physics, IIT Bombay, Powai, Mumbai-400076, India*
[d]*Graduate School of Flexible & Printable Electronics Engineering, Chonbuk National University, Jeonju, Jeonbuk 561-756, Korea*
[e]*Solar Energy Material Laboratory, Department of Energy, Tezpur University, Tezpur, Assam 784 028, India*
[f]*Department of Physics & Astrophysics, University of Delhi, Delhi-110007, India*
[g]*Department of Applied Chemistry, Delhi Technological University, Shahbad Daulatpur, Main Bawana Road, Delhi-110042, India*
†Electronic supplementary information (ESI) available. See DOI: 10.1039/c5nr02837j

the gas molecules and restricted diffusion in the boundaries result in low sensitivity and poor selectivity for target gases. To resolve this critical problem, different types of MOS/RGO based nanocomposites have been developed. Decoration of RGO with metal oxide nanocrystals promotes charge transfer between specific gas species, which has proven to be an effective way to improve the sensitivity, and achieve faster response/recovery and better selectivity for the specific gas at a particular operating temperature.

Hydrogen (H_2) is an invisible, odorless and flammable gas for which safety becomes a primary concern, since the presence of H_2 concentration in excess of 4 vol% in the environment is potentially explosive.[27] On the other hand, liquefied petroleum gas (LPG), mainly a mixture of propane and butane is a highly inflammable gas which is regularly used in automobiles and industry and for other domestic purposes.[28] LPG is most commonly used in the kitchen as cooking fuel but bears high possibility of explosion accidents due to leakage/human error or bursting of LPG filled cylinders. A small leakage may be more dangerous for living bodies as well as domestic and industrial properties. Hence, it is very important to monitor these gases in the environment and working places at its early stages to raise alarm and perform effective suppression.

Numerous efforts have been made towards the development of different types of gas sensors using nanostructure materials. Liu *et al.* studied a flexible, rapid-response gas sensor based on colloidal quantum dot solids.[29] They have demonstrated a high performance, paper-based flexible NO_2 gas sensor using PbS CQDs. Xu *et al.* reported the fabrication of a SnO_2-RGO monolayer-ordered porous film gas sensor with tunable sensitivity through ultra-violet light irradiation.[30] Nemade *et al.* synthesized graphene/SnO_2 QDs through an *in situ* synthesis method and investigated chemiresistive gas sensing.[31] Inyawilert *et al.* studied a rapid ethanol sensor based on electrolytically-exfoliated graphene loaded with a flame-made In-doped SnO_2 composite film.[32] These authors have investigated that the graphene (5 wt%) when composed with 0.5 wt% In-doped SnO_2 led to a drastic enhancement of response (965) along with a very short response time (1.8 s) and fast recovery stabilization at an optimal operating temperature of 350 °C. Lee *et al.* reported a novel approach to enhance the gas sensing properties of n-type nanofibers that involves the formation of p–n hetero-junctions with p-type RGO nanosheets.[33] Li *et al.* have developed a 3D-SnO_2/RGO nanocomposite as a high performance NO_2 gas sensor at low operating temperatures.[34] The CO gas sensing properties of the direct-patternable SnO_2 thin films containing graphene or Ag nanoparticles have been studied by H. Kim *et al.*[35] Singkammo *et al.* investigated graphene loaded with a flame-made Ni-doped SnO_2 composite film for acetone sensing.[36] Recently, Liu *et al.* studied the chemiresistive gas sensors employing solution-processed metal oxide quantum dot films.[37] They have studied the detection limit of the gas sensor and observed that it was down to 6 ppb.

Herein, we studied the possibilities to detect H_2 and LPG by the RGO/SnO_2 QD based sensing element synthesized by an *in situ* assisted hydrothermal method. Further, we have investigated the synergetic effect of RGO and SnO_2 QDs on the sensing properties of H_2 and LPG. Here, the amount of RGO (1.0 mg in the present study) plays a vital role in improving the sensing characteristics as a combination of higher sensor response magnitude, good selectivity, excellent sensor reproducibility and short response/recovery time. The decoration of nano-sized SnO_2 QDs on the RGO surface was selected for this study for several reasons such as zero dimensions, high surface to volume ratio, low operating temperature and low test gas concentrations compared to other conventional sensors. High response, good selectivity and excellent reproducibility of this sensor as well as faster response and recovery to H_2 and LPG exposure can have a significant importance in the domestic and industrial applications.

Experimental details

Graphite was purchased from Alfa Aesar whereas glucose was obtained from Merck and used without further purification. Unless otherwise stated, other reagents were of analytical grade and used as received. All aqueous solutions were prepared with ultrapure water (>18 MΩ) from a Milli-Q Plus system (Millipore).

RGO was synthesized from graphite powder following the modified Hummers method.[24] The RGO/SnO_2 QDs were prepared by the hydrothermal method. In this process firstly, 10 mmol of $SnCl_4{\cdot}5H_2O$ was dissolved in distilled water to form a transparent colorless solution and then 1.0 mg RGO was added to the above solution. Subsequently, with mild stirring, 1 ml hexamethyldisilazane (HMDS) surfactant was added to the above solution. Next, the pH was maintained at 8.5 by adding a NaOH solution dropwise into the above solution. The whole solution was transferred into a 100 ml Teflon-lined stainless steel autoclave to react at 120 °C for 20 h and then allowed to cool naturally to room temperature. The obtained precipitate was separated by centrifuging at 4000 rpm for 30 minutes and washed with distilled water and ethanol several times to remove impurity ions and dried at 60 °C for 3 hours in a hot air oven. The precipitate was then calcined at 400 °C for 1 hour to obtain the final products of RGO/SnO_2 nanocomposites. The same experimental process was performed to prepare pure SnO_2 QDs. The dried mass was then crushed into fine powder for further characterization. The fine powder of RGO/SnO_2 QD nanocomposites, RGO and SnO_2 QDs were pressed into pellets of 10.5 mm diameter and 1.0 mm thickness at a pressure of ~15 MPa using a hydraulic press. These pellets were further sintered at 150 °C for 30 minutes. After that, high-temperature silver paste was used for making the ohmic contacts on both surfaces of the pellet.

The shape and size of the as-prepared RGO/SnO_2 QDs were investigated by high resolution transmission electron microscopy (HR-TEM) on a Philips model Tecnai-20 using an accelerating voltage of 200 kV. Raman spectroscopy was

performed using the Lab RAM HR 800 Microlaser Raman system in backscattering geometry using the 514.5 nm line of an Ar^{+}-laser as an excitation source. The detailed characterization of RGO/SnO_2 QD, RGO and SnO_2 QD samples with gas sensing properties is performed and presented in the ESI.† In the present study, the H_2 and LPG sensor responses of RGO/SnO_2 QDs have been calculated using the following equation.[28]

$$S(\%) = \frac{R_a - R_g}{R_a} \times 100 \quad (1)$$

where R_g is the resistance of the sensor device (pellet) in the presence of gas and R_a is the background resistance in the presence of air.

Results and discussion

Structural studies

XRD spectra of RGO/SnO_2 QDs and SnO_2 QDs depict the tetragonal crystal structure of SnO_2 QDs with (110), (101), (211) and (112) diffraction planes which is consistent with JCPDS card no. 72-1147 [Fig. S1(a and c)†] whereas a broad peak observed at $2\theta = 24.2775°$ (d-spacing = 0.37 nm) is attributed to the (002) plane of RGO [Fig. S1(a and b)†]. The elemental analysis of the RGO/SnO_2, RGO and SnO_2 QDs has been performed by XPS [Fig S2(a–c)†]. TEM, HR-TEM and selected area electron diffraction pattern (SAED) micrographs of RGO/SnO_2 QDs are presented in Fig. 1(a–d), to explore the structure, defects and lattice fringes. TEM images [Fig. 1(a and b)] undoubtedly indicated that the dark spots on the surface of RGO are composed of SnO_2 QDs. The SnO_2 QDs decorated on the RGO surface have also prevented the RGO from re-stacking into a multilayer.[38,39] The size of the SnO_2 QDs is ~6 nm and shows good distribution over the RGO [Fig. 1(a and b)].

The HR-TEM image [Fig. 1(c)] shows the lattice spacing and the corresponding planes of RGO/SnO_2 QDs. The lattice spacing of RGO is observed to be 0.37 nm corresponding to the (002) plane whereas SnO_2 QDs have a d-spacing of 0.32 nm corresponding to the (110) plane. In Fig. 1(d), the SAED pattern reveals well-defined circular rings, suggesting the polycrystalline nature of the as synthesized RGO/SnO_2 QDs. These rings could be indexed to the (110), (101), (200), (211) & (112) planes of the SnO_2 phase whereas the dotted ring corresponds to the (200) plane of RGO.[40,41] The above result clearly suggests good polycrystallinity of RGO/SnO_2 QDs. It can also be seen that each SnO_2 QD is attached to several other quantum dots and well dispersed on the surface of RGO [Fig. 1(a and b)]. Thus, good contact between the SnO_2 QDs and RGO can effectively minimize the electrical isolation of the nanostructure during the gas sensing test. RGO with higher surface area loaded with SnO_2 QDs can offer an improved conducting network that could facilitate electron transfer during the chemisorption process of the gas sensing. The TEM and HRTEM images of bare RGO and SnO_2 QD samples are also investigated and shown in Fig. S3(a and b).† The FE-SEM and the corresponding elemental mapping images are presented in Fig. S4(a–c).† The UV-Vis studies have been performed to investigate the quantum dot nature of RGO/SnO_2 QD and SnO_2 QD samples [Fig. S5(a and b)†].

Raman spectroscopy is a powerful technique to characterize the RGO based material, particularly the order/disorder and defect characteristics. Fig. 2 shows Raman spectra of the as-prepared RGO/SnO_2 QDs. The characteristic Raman bands of RGO are observed at ~1353 cm^{-1} (k-point phonons of A_{1g} symmetry, D band) and ~1579 cm^{-1} (E_{2g} phonons of sp^2 atoms, G band). The G band (~1579 cm^{-1}) is related to the

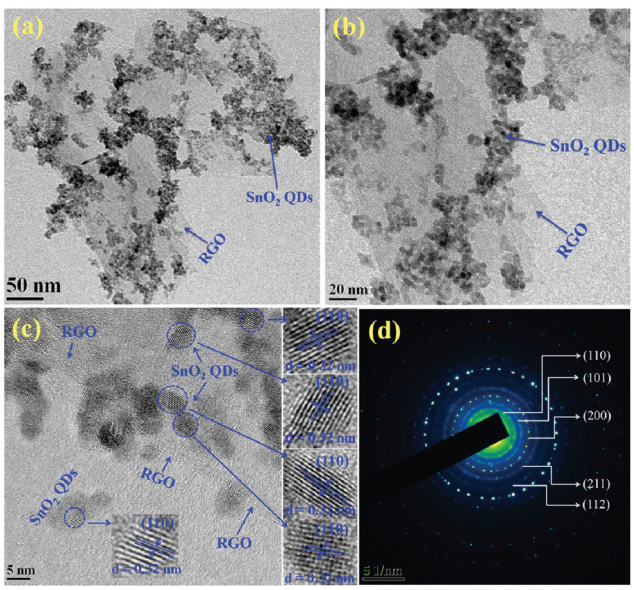

Fig. 1 (a and b) TEM, (c) HR-TEM and (d) SAED images of RGO/SnO_2 QDs.

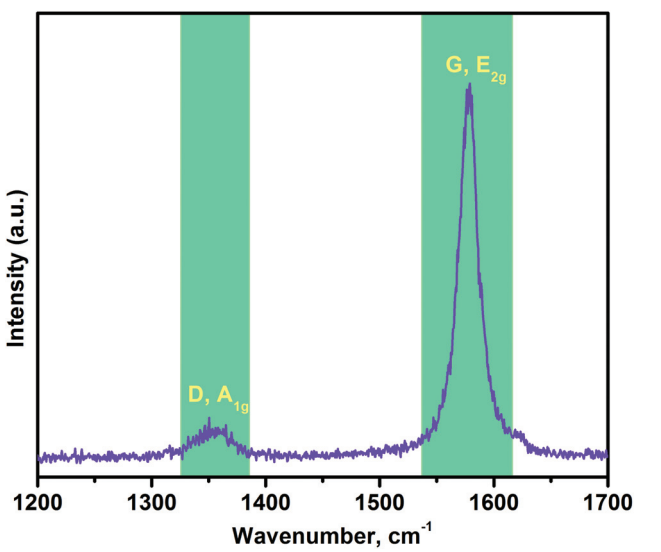

Fig. 2 Raman spectrum of RGO/SnO_2 QDs.

in-plane vibration of sp^2-bonded carbon atoms whereas the D Raman band (~1348 cm^{-1}) could be related to the breathing mode of the rings of sp^2-hybridized carbon.[42,43] The D band indicates the presence of defect in RGO/SnO_2 QDs which may be associated with vacancies, grain boundaries, amorphous carbon species and disorder in the hexagonal graphitic layer.[44]

The Raman spectrum of RGO/SnO_2 QDs shows an intense G band whereas a D band of very low intensity, indicating low degree of defect in RGO. Therefore, we can say that some of these defect states arising due to nucleation centers, *i.e.* where the growth is initiated, reflects an elastic intervalley scattering process.[45] The existence of both G and D bands confirms the presence of RGO in the composite. The negligible intensity ratio of I_D/I_G suggests that the C=C bonds at the RGO surface are damaged in the hydrothermal synthesis process, followed by adsorption of SnO_2 QDs on the surface of RGO which reduced the number of oxygen-containing functional groups.[40]

Gas sensing studies

H_2 and LPG sensing study

The H_2 and LPG gas sensing experiments were performed at different operating temperatures (150–275 °C) in order to examine the most favorable working temperature for H_2 and LPG gas recognition. All the gas sensing experiments were carried out at a relative humidity of ~43% under atmospheric pressure.

To avoid the interference of humidity with the sensor performance, at each particular operating temperature, the sensing element was allowed to equilibrate inside the static test gas chamber for 30 minutes before exposing to the H_2 and LPG gas. The H_2 and LPG gas sensing and the presence in different interfering vapor schematic test chambers were reported elsewhere.[10,28] A number of experiments have been carried out to investigate the test gas responses for various concentrations (100–500 ppm) as a function of operating temperature. The gas sensing properties of the RGO/SnO_2 QD based sensor strongly depends on the temperature as well as the test gas concentration. Thus the response of the RGO/SnO_2 QD based sensor as a function of operating temperature is mainly governed by RGO and SnO_2 QD surface stoichiometry and analyte–surface chemical interactions. In order to evaluate the test gas response of the RGO/SnO_2 QD sensor, the change in electrical resistance was measured upon exposure to various test gas concentrations at different operating temperatures, which can be explained by a dynamic equilibrium state of adsorption and desorption.

Fig. 3(a and b) show H_2 and LPG sensing response characteristics of the RGO/SnO_2 QDs as a function of operating temperature (150–275 °C) for various test gas concentrations (100–500 ppm), respectively. As shown in Fig. 3(a), the response increases for all H_2 gas concentrations up to an operating temperature of 200 °C and found to be maximum (89.3%), after that the sensor response was observed to be

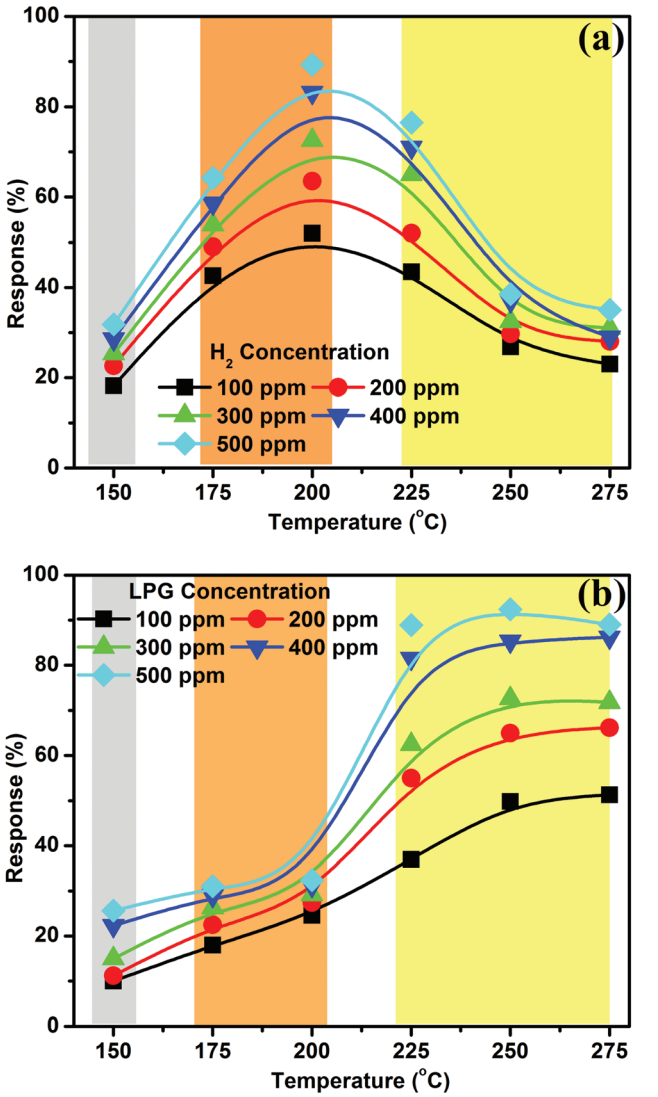

Fig. 3 Response curve of the RGO/SnO_2 QD based H_2 (a) and LPG (b) sensor as a function of operating temperature for various test gas concentrations.

decreased. The increase in sensing response may perhaps be due to the lattice strain/structural deformation and high surface to volume ratio of SnO_2 QDs & RGO. Therefore, more adsorption sites are available for the adsorption of O_2 molecules on the surface of the RGO/SnO_2 QDs, resulting in higher response. It is expected that the presence of structural defects and oxygen vacancies in the RGO/SnO_2 QDs is more favorable for the adsorption of atmospheric oxygen on the surface of the RGO/SnO_2 QD sensor, leading to higher gas response. On the other hand, the response was found to be decreased with increasing temperatures beyond 200 °C. The decrease in response at higher operating temperatures is attributed to the non-availability of sufficient sensing sites on the RGO/SnO_2 QD surface, which may arise due to the deficiency of adsorbed atmospheric oxygen on the sensor surface. In other words, it

may be due to the less interaction of the test gas with the active sites present on the sensor surface or the very poor concentration of electrons in the conduction band which interact with the atmospheric oxygen species to form active sites O^-, which is completely responsible for the gas sensing mechanism.

The changes in the gas sensing response at different operating temperatures over increased LPG concentrations have been investigated and the results are presented in Fig. 3(b). It is observed that at low operating temperatures (<200 °C) the LPG response is slow, since gas molecules do not have enough thermal energy to react with the surface adsorbed oxygen species. In fact, a potential barrier to charge transport is formed during adsorption of atmospheric oxygen on the surface or this may be due to the low diffusion or interaction of LPG molecules with RGO/SnO_2 QDs at moderate temperature. However, at higher temperatures (>225 °C) the LPG response reaches its maximum response of ~92.4% at 250 °C above which the LPG response attains saturation. This may be due to the more test gas injection leading to the higher gas sensing response of the RGO/SnO_2 QD sensor, which might be accredited to higher surface coverage and thus more surface reaction takes place.

In other words, we can say that at an operating temperature of 150 °C, the sensing response increases for all concentrations and found to be maximum ~31.8% for H_2 [Fig. 3(a)] and ~25.6% for LPG [Fig. 3(b)] at 500 ppm concentration. This phenomenon may be attributed to the higher surface to volume ratio of the RGO supported SnO_2 QDs. The gas response increases rapidly between 175 °C and 200 °C for all concentrations and reaches its maximum response of ~89.3% for 500 ppm concentration to H_2 [Fig. 3(a)]. This may be due to the increased conductivity which is attributed to the thermal excitation of electrons into the conduction band of the RGO/SnO_2 QDs. However, as shown in Fig. 3(b), the response to LPG is very poor in the same temperature range. Here, the LPG molecules may not have sufficient thermal energy to dissociate into its constituents to interact with active sites O^- at that particular temperature, resulting in low gas response. However, at higher operating temperatures (225 °C to 275 °C), the thermal excitation of electrons and oxygen adsorption occur simultaneously[46] which play a vital role in both H_2 and LPG response. In Fig. 3(a), for all test concentrations the H_2 response decreases with operating temperature. Here, the oxygen adsorption/desorption process may be dominant over the thermal excitation of electrons, therefore the response tends to decrease. But in the case of LPG, the thermal excitation of electrons may be dominant over the oxygen adsorption/desorption process resulting in higher response as shown in Fig. 3(b).[47]

The gas sensing results of RGO and SnO_2 QDs towards H_2 and LPG have also been investigated at the same operating temperature and concentration range and are presented in the ESI (Fig. S6 and Fig. S7†). It is observed that the gas sensing response of the RGO/SnO_2 QD based H_2 and LPG sensor is superior to that of bare RGO and SnO_2. This improved sensing performance of RGO/SnO_2 QDs is attributed to the synergetic effect between the RGO and SnO_2 QDs.

Thus, the optimum working temperature for the RGO/SnO_2 QDs to recognize the 500 ppm concentration of H_2 and LPG is 200 °C and 250 °C, respectively, which are modest from the viewpoint of gas sensors. Hence, the optimum working temperatures of 200 °C and 250 °C have been chosen in order to study the H_2 and LPG sensing properties such as response, selectivity, reproducibility and response/recovery times.

H_2 and LPG sensing mechanism

The H_2 and LPG sensing mechanism of RGO/SnO_2 QDs is a surface controlled process. It is based on the changes in the electrical resistance of RGO/SnO_2 QDs which is controlled by the LPG and H_2 species and the amount of the chemisorbed oxygen on the surface of the sensor. The adsorption of the test gases, which depends on both the type of the test gas and the sensor material, affects both the response characteristics and response/recovery times. With increasing operating temperature, atmospheric oxygen is adsorbed on the surface and grain boundaries and then it exists in various forms. The adsorption of atmospheric oxygen species on the sensor surface forms ionic species such as O_2^- and O^- which acquire electrons from the conduction band of the sensing material, and this helps in understanding the gas sensing mechanism of the RGO/SnO_2 QD based H_2 and LPG sensor. The reaction kinetics between atmospheric oxygen and the RGO/SnO_2 QD sensor surface is as follows:[10]

$$O_2(\text{air}) \Leftrightarrow O_2(\text{ads}) \quad (2a)$$

$$O_2(\text{ads}) + e^- \Leftrightarrow O_2^-(\text{ads}) \quad (2b)$$

$$O_2^-(\text{ads}) + e^- \Leftrightarrow 2O^-(\text{ads}) \quad (2c)$$

Thus, the immobility of the chemisorption process results in the stabilization of the sensor surface resistance. Other internal or external factors that affect the chemisorption process give rise to electrical resistance.

On injecting the reducing H_2 gas into the test chamber, the H_2 molecules react with the active sites O^- which are available on the surface of the RGO/SnO_2 QD sensor and release electrons back into the lattice tending to decrease the sensor resistance. The H_2 sensing reaction mechanism has been discussed in the earlier study.[48]

$$H_2 + O^-(\text{ads}) \rightarrow H_2O + e^- \quad (3)$$

However, the LPG sensing mechanism is a complex process and it is believed that it proceeds through several intermediate steps which are not yet understood. The reaction mechanism of LPG with chemisorbed active site O^- can be written as follows:[28]

$$C_nH_{2n+2} + 2O^- \rightarrow C_nH_{2n} : O + e^- + H_2O \quad (4a)$$

$$C_nH_{2n} : O + O^- \rightarrow CO_2 + H_2O + e^- \quad (4b)$$

where C_nH_{2n+2} stands for CH_4, C_3H_8, C_4H_{10}, *etc.*, while C_nH_{2n}: O represents partially oxidized intermediates on the RGO/SnO_2 QD surface.

Selectivity study of H_2 and LPG sensor

Apart from sensitivity, selectivity is an important parameter for gas sensors. The gas responses towards a specific test gas for the same concentration are required to be noticeably higher than those to other interfering gases for selective gas detection. In the present study, the interfering gases such as ammonia, chloroform, toluene, benzene, acetone, *n*-butylacetate, acetic acid and formic acid have been used to study the selective behavior of the RGO/SnO_2 QD based H_2 and LPG sensor. Fig. 4(a and b) show the selective responses of the RGO/SnO_2 QD based H_2 and LPG sensor towards different interfering gases for fixed 500 ppm concentration at operating temperatures of 200 °C and 250 °C, respectively. The RGO/SnO_2 QD based sensor exhibits selectively higher response for 500 ppm concentration to H_2 (~89.3%) at an operating temperature of 200 °C whereas it shows a significantly lower response (~3%) to acetic acid, ammonia, chloroform, toluene, benzene, *n*-butylacetate, acetone and formic acid as shown in Fig. 4(a).

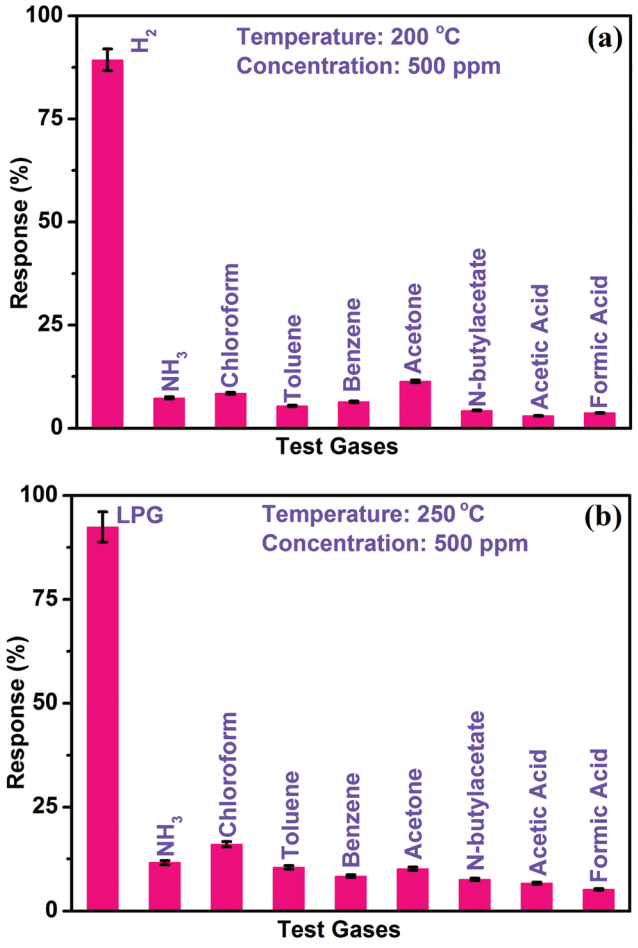

Fig. 4 Bar chart shows selective response of the RGO/SnO_2 QD based sensor. The gas concentration and operating temperature in all cases were 500 ppm and 200 °C for H_2 (a) whereas 250 °C for LPG (b) selective gas detection, respectively.

On the other hand, the RGO/SnO_2 QD sensor also exhibits high selective performance for 500 ppm concentration to LPG (~92.4%) at an operating temperature of 250 °C compared to a very low response (5.2%) to formic acid, chloroform, ammonia, toluene, benzene, acetone, *n*-butylacetate and acetic acid as presented in Fig. 4(b). The highest response of the RGO/SnO_2 QD based sensor towards H_2 and LPG has been observed at optimum working temperatures 200 °C and 250 °C, respectively, and nearly no response to the interfering gases [Fig. 4(a and b)]. This phenomenon can be explained on the basis of the change of the resistance of the sensor caused by the charge transfer between RGO/SnO_2 QDs and target molecules that exhibit very good H_2 and LPG gas diffusivity and also good interaction with RGO and SnO_2 QDs rather than other interfering gases.

In order to quantify the selectivity for H_2 and LPG, the selectivity coefficient (K_{sc}) of H_2 and LPG for other interfering gases has been calculated using the following equation:[49]

$$K_{sc} = \frac{S_{H_2,LPG}}{S_{gas}} \quad (5)$$

where $S_{H_2,\ LPG}$ and S_{gas} are the responses of the sensor to H_2 & LPG and other interfering target gases, respectively, as listed in Table 1.

The selectivity coefficient "K_{sc}" for the RGO/SnO_2 QD based H_2 sensor operated at 200 °C for 500 ppm concentration is the highest for acetic acid (29.8) whereas for the RGO/SnO_2 QD nanocomposite based LPG sensor operated at 250 °C for the same concentration it was found to be maximum for formic acid (17.8). The higher values of K_{sc} show the more selective detection to H_2 and LPG for 500 ppm concentration at optimum working temperatures of 200 °C and 250 °C, respectively. For example, the value of K_{sc} = 29.8 for acetic acid suggests that the gas response to H_2 is 29.8 times higher than that to acetic acid whereas K_{sc} = 17.8 for formic acid reveals that the gas response to LPG is 17.8 times higher than that to formic acid. Thus our experimental findings indicate that the RGO/SnO_2 QD based sensor has a good selectivity for H_2 and LPG for 500 ppm concentration at optimum working temperatures of 200 °C and 250 °C, respectively. Based on the experimental observations, it can be concluded that the formation of SnO_2 QDs on RGO is not only effective to improve the H_2 and LPG responses but also makes it efficient for detection of H_2 and LPG.

Long-term reproducibility study of H_2 and LPG sensor

In practical applications, besides sensitivity and selectivity, long-term reproducibility of the gas sensor is also critical for which we must determine the consistency of the gas sensor over its period of service. To justify the reproducible nature with which the RGO/SnO_2 QD sensor shows maximum response, the gas response measurements were tested at optimum

Table 1 The selectivity coefficient "K_{sc}" of the RGO/SnO_2 QD based H_2 and LPG sensor for different interfering gases for 500 ppm concentration at optimum working temperatures of 200 °C and 250 °C, respectively

	Interfering gases with concentration of 500 ppm							
Sensing system	Ammonia	Chloroform	Toluene	Benzene	Acetone	*N*-Butylacetate	Acetic acid	Formic acid
RGO/SnO_2 QD based H_2 sensor (200 °C)	12.2	10.6	16.5	13.9	7.9	20.8	29.8	24.1
RGO/SnO_2 QD based LPG sensor (250 °C)	7.9	5.8	8.8	11.0	9.1	12.2	13.8	17.8

working temperatures of 200 °C and 250 °C for 500 ppm concentration to the H_2 and LPG, respectively.

From the initial day to 50 days later, the response changed slightly by −4% to H_2 and −3% to LPG, demonstrating good reproducibility of the sensor as shown in Fig. 5(a and b). It has also been observed that the gas response increases sharply with insertion of H_2 and LPG and returns to its original state when the test gas is left out. This behavior is attributed to good electrical properties and high surface area of RGO/SnO_2 QDs, to interact with test gas. In addition, the rate of adsorption–desorption increases at that working temperature due to the increased diffusivity of gases at high temperatures, leading to a large number of depleted grains. Our findings conclude that RGO supported SnO_2 QDs have excellent reproducibility. However, the reproducibility mechanism is more complicated, and further analyses are required to gain a good understanding.

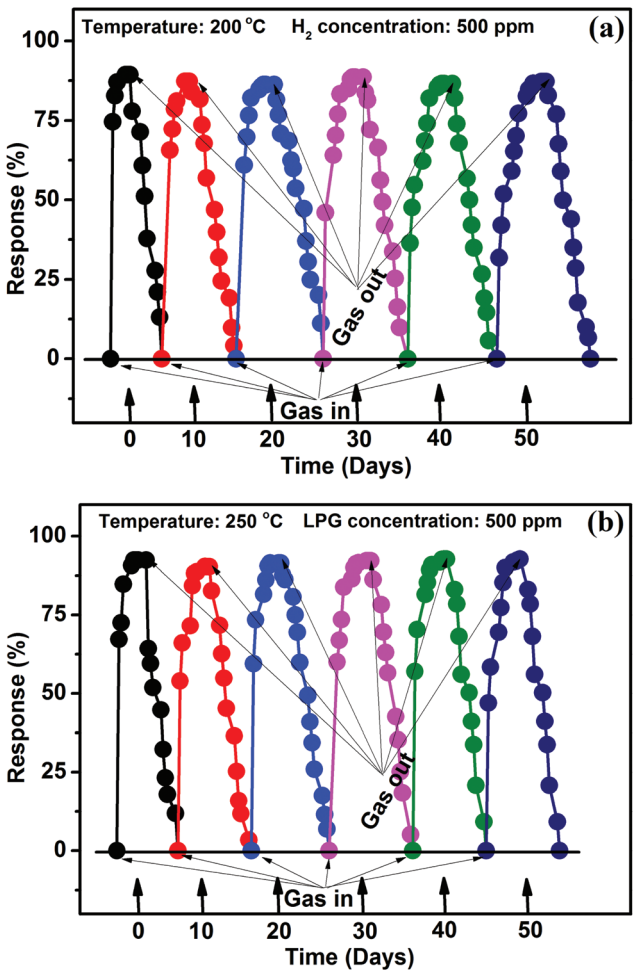

Fig. 5 Long term reproducible nature of the RGO/SnO_2 QD sensor at operating temperatures 200 °C and 250 °C for 500 ppm concentration to the H_2 (a) and LPG (b), respectively.

Real-time analyses of H_2 and LPG sensor

The response/recovery real-time study is an important characteristic for evaluating the performance of gas sensors. The response time is typically defined as the time taken by a sensor to read a certain percentage of full-scale reading (normally 90%) when exposed to a test gas. Similarly, the recovery time is the time taken by the sensor to return to its original state when the test gas is removed.

Fig. 6(a and b) show the response/recovery real time plot of the RGO/SnO_2 QDs to H_2 and LPG in the concentration range of 100–500 ppm at operating temperatures of 200 °C and 250 °C, respectively. It has been observed that with increasing test gas concentrations, the response time decreases which is due to increased surface coverage of the test gas molecules, resulting in the quick reaction of H_2 and LPG molecules with adsorbed atmospheric oxygen species. At lower test gas concentrations, the response times are more compared to recovery times because the sensor surface is insufficiently covered with the test gas molecules and therefore the reaction slows down.

It has also been noticed that LPG has low response recovery times compared to H_2 except at 500 ppm concentration. This may be due to the sufficient thermal energy to excite the electrons from the valence band to the conduction band which provides more sensing sites at 250 °C compared to 200 °C. Here, it has also been observed that the gas sensing response time decreases with increasing H_2 concentration [Fig. 6(a)] whereas in the case of LPG [Fig. 6(b)] the response time first increases and then decreases. It may be due to the more complex sensing mechanism of LPG which dissociates into its constituents through several intermediate steps compared to H_2, as presented in eqn (4a), (4b) and (3), respectively. In other words, we can say that the sensor temperature also regulates the activation energies of the adsorption–desorption and thereby the kinetics of surface chemisorption reaction, which is reflected in the response and recovery times of the sensor signal.

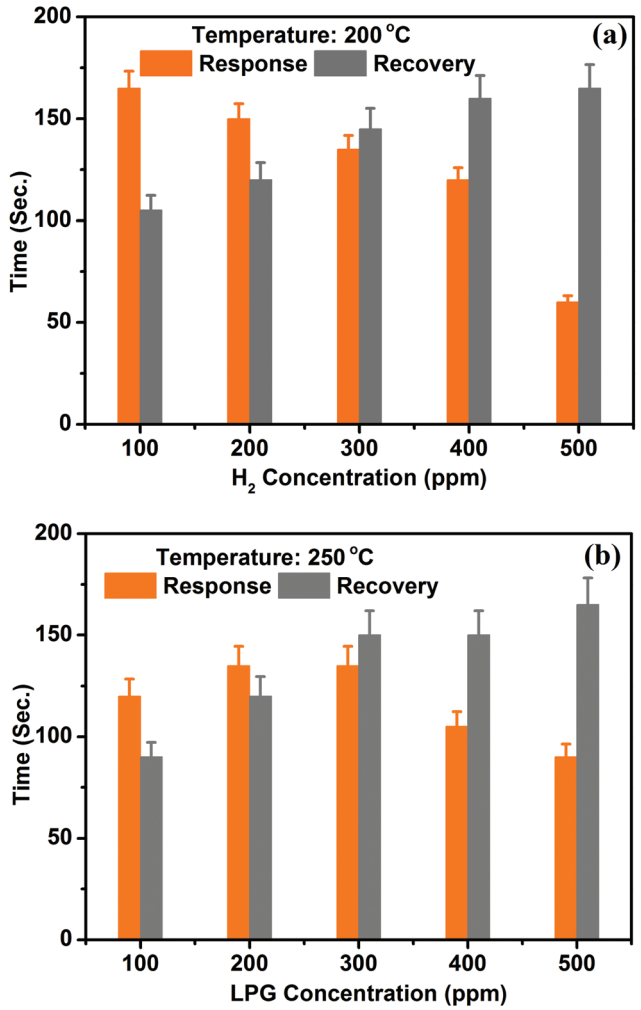

Fig. 6 The response/recovery real time plot of the RGO/SnO_2 QD sensor to H_2 (a) and LPG (b) in the concentration range 100–500 ppm at operating temperatures of 200 °C and 250 °C, respectively.

Specifically, the presence of the SnO_2 QDs on the surface or into the lattice structure of RGO promotes the formation of a potential barrier between the interfaces of the two materials, which governs the electron transport properties of the nanomaterials. It may be caused by the difference in the work function of the different materials. Therefore, response and recovery times are affected correspondingly.

Thus, our experimental results of gas sensing properties reveal that the RGO/SnO_2 QDs have good H_2 and LPG sensing properties such as higher gas response, good selectivity, short response/recovery times and excellent reproducibility at lower operating temperatures.

Conclusions

In conclusion, the SnO_2 QDs decorated on RGO have been successfully synthesized by the hydrothermal method. Structural, morphological, elemental, optical and defect studies of the as prepared RGO/SnO_2 QDs were carried out by XRD, XPS, HR-TEM, FE-SEM, UV-Vis spectroscopy and Raman spectroscopy techniques. UV-Vis spectroscopy suggested the quantum confinement feature of the as-synthesized RGO/SnO_2 QDs [Fig. S5†]. The HR-TEM study revealed that SnO_2 QDs with a size less than 6 nm were anchored on the surface of RGO. The RGO/SnO_2 QD based sensor is demonstrated for H_2 and LPG gas detection for 500 ppm concentration at optimum working temperatures of 200 °C and 250 °C, respectively. Its high and fast response/recovery times as well as good sensitivity, selectivity and reproducibility make it a potential candidate for high performance H_2 and LPG sensors.

Acknowledgements

The authors are highly grateful to Professor M. Aslam, Department of Physics, Indian Institute of Technology Bombay, India, for providing TEM and Raman facilities. Further, the authors wish to express gratitude to the SAIF IIT Bombay, India, for TEM and Raman measurements. The authors are grateful to Chonbuk National University, South Korea, for providing characterization facility of other samples. The authors are also thankful to the Regional Innovation Center for Next Generation Industrial Radiation Technology, Wonkwang University, South Korea, for providing XPS facility. This research was supported by the Basic Research Laboratory Program (2014R1A4A1008140) through the Ministry of Science, ICT & Future Planning and through the National Research Foundation of Korea (NRF) funded by Ministry of Education and Polymer Materials Fusion Research Center. MS acknowledges the DST, Government of India for a DST-INSPIRE Fellowship [IFA13-MS-02] 2014. JS acknowledges the DST, Government of India for a DST-INSPIRE Fellowship [IFA-13 CH-105] in 2013 and a DST Young Scientist award (CS-393/2012).

References

1 F. Schedin, A. K. Geim, S. V. Morozov, E. W. Hill, P. Blake, M. I. Katsnelson and K. S. Novoselov, *Nat. Mater.*, 2007, **6**, 652–655.
2 P. T. Moseley, *Meas. Sci. Technol.*, 1997, **8**, 223–237.
3 J. Wu, M. Agrawal, H. A. Becerril, Z. Bao, Z. Liu, Y. Chen and P. Peumans, *ACS Nano*, 2010, **4**, 43–48.
4 S. Kumar and J. Koh, *Int. J. Biol. Macromol.*, 2014, **70**, 559–564.
5 Y. Pak, S.-M. Kim, H. Jeong, C. G. Kang, J. S. Park, H. Song, R. Lee, N.-S. Myoung, B. H. Lee, S. Seo, J. T. Kim and G.-Y. Jung, *ACS Appl. Mater. Interfaces*, 2014, **6**, 13293–13298.
6 W. Yuan, L. Huang, Q. Zhou and G. Shi, *ACS Appl. Mater. Interfaces*, 2014, **6**, 17003–17008.
7 Q. Huang, D. Zeng, H. Li and C. Xie, *Nanoscale*, 2012, **4**, 5651–5658.

8 D. Zhang, A. Liu, H. Chang and B. Xi, *RSC Adv.*, 2015, **5**, 3016–3022.
9 A. Kaniyoor, R. I. Jafri, T. Arockiadoss and S. Ramaprabhu, *Nanoscale*, 2009, **1**, 382–386.
10 R. K. Mishra, A. Kushwaha and P. P. Sahay, *RSC Adv.*, 2014, **4**, 3904–3912.
11 J. Jeong, S.-P. Choi, C. I. Chang, D. C. Shin, J. S. Park, B. T. Lee, Y.-J. Park and H.-J. Song, *Solid State Commun.*, 2003, **127**, 595–597.
12 Y. Cheng, P. Xiong, C. S. Yun, G. F. Strouse, J. P. Zheng, R. S. Yang and Z. L. Wang, *Nano Lett.*, 2008, **8**, 79–84.
13 H. Lee, C.-M. Kang, M. Park, J. Kwak and C.-h. Lee, *ACS Appl. Mater. Interfaces*, 2013, **5**, 1977–1981.
14 J. T. Park, C. S. Lee and J. H. Kim, *Nanoscale*, 2015, **7**, 670–678.
15 J. Yan, E. Khoo, A. Sumboja and P. S. Lee, *ACS Nano*, 2010, **4**, 4247–4255.
16 J. Lin, Z. Peng, C. Xiang, G. Ruan, Z. Yan, D. Natelson and J. M. Tour, *ACS Nano*, 2013, **7**, 6001–6006.
17 C. Dong, X. Liu, X. Xiao, G. Chen, Y. Wang and I. Djerdj, *J. Mater. Chem. A*, 2014, **2**, 20089–20095.
18 A. K. Geim and K. S. Novoselov, *Nat. Mater.*, 2007, **6**, 183–191.
19 X. Kang, J. Wang, H. Wu, J. Liu, I. A. Aksayc and Y. Lin, *Talanta*, 2010, **8**, 754–759.
20 K. S. Novoselov, A. K. Geim, S. V. Morozov, D. Jiang, Y. Zhang, S. V. Dubonos, I. V. Grigorieva and A. A. Firsov, *Science*, 2004, **306**, 666–669.
21 A. Ismach, C. Druzgalski, S. Penwell, A. Schwartzberg, M. Zheng, A. Javey, J. Bokor and Y. Zhang, *Nano Lett.*, 2010, **10**, 1542–1548.
22 C. Berger, Z. M. Song, T. B. Li, X. B. Li, A. Y. Ogbazghi, R. Feng, Z. T. Dai, A. N. Marchenkov, E. H. Conrad, P. N. First and W. A. de Heer, *J. Phys. Chem. B*, 2004, **108**, 19912–19916.
23 A. Srivastava, C. Galande, L. Ci, L. Song, C. Rai, D. Jariwala, K. F. Kelly and P. M. Ajayan, *Chem. Mater.*, 2010, **22**, 3457–3461.
24 C. Zhu, S. Guo, Y. Fang and S. Dong, *ACS Nano*, 2010, **4**, 2429–2437.
25 Y. Shao, J. Wang, M. Engelhard, C. Wang and Y. Lin, Facile and controllable electrochemical reduction of graphene oxide and its applications, *J. Mater. Chem.*, 2010, **20**, 743–748.
26 T. H. Seo, T. S. Oh, S. J. Chae, A. H. Park, K. J. Lee, Y. H. Lee and E.-K. Suh, *Jpn. J. Appl. Phys.*, 2011, **50**, 125103.
27 C.-M. Chang, M.-H. Hon and I.-C. Leu, *ACS Appl. Mater. Interfaces*, 2013, **5**, 135–143.
28 R. K. Mishra and P. P. Sahay, *Mater. Res. Bull.*, 2012, **47**, 4112–4118.
29 H. Liu, M. Li, O. Voznyy, L. Hu, Q. Fu, D. Zhou, Z. Xia, E. H. Sargent and J. Tang, *Adv. Mater.*, 2014, **26**, 2718–2724.
30 S. Xu, F. Sun, S. Yang, Z. Pan, J. Long and F. Gu, *Sci. Rep.*, 2015, **5**, 8939.
31 K. R. Nemade and S. A. Waghuley, *Mater. Sci. Semicond. Process.*, 2014, **24**, 126–131.
32 K. Inyawilert, A. Wisitsoraat, C. Sriprachaubwong, A. Tuantranont, S. Phanichphant and C. Liewhiran, *Sens. Actuators, B*, 2015, **209**, 40–55.
33 J.-H. Lee, A. Katoch, S.-W. Choi, J.-H. Kim, H. W. Kim and S. S. Kim, *ACS Appl. Mater. Interfaces*, 2015, **7**, 3101–3109.
34 L. Li, S. He, M. Liu, C. Zhang and W. Chen, *Anal. Chem.*, 2015, **87**, 1638–1645.
35 H. Kim, C.-S. Park, K.-M. Kang, M.-H. Hong, Y.-J. Choi and H.-H. Park, *New J. Chem.*, 2015, **39**, 2256–2260.
36 S. Singkammo, A. Wisitsoraat, C. Sriprachuabwong, A. Tuantranont, S. Phanichphant and C. Liewhiran, *ACS Appl. Mater. Interfaces*, 2015, **7**, 3077–3092.
37 H. Liu, S. Xu, M. Li, G. Shao, H. Song, W. Zhang, W. Wei, M. He, L. Gao, H. Song and J. Tang, *Appl. Phys. Lett.*, 2014, **105**, 163104.
38 Z. F. Du, X. M. Yin, M. Zhang, Q. Y. Hao, Y. G. Wang and T. H. Wang, *Mater. Lett.*, 2010, **64**, 2076–2079.
39 P. C. Lian, X. F. Zhu, H. F. Xiang, Z. Li, W. S. Yang and H. H. Wang, *Electrochim. Acta*, 2010, **56**, 834–840.
40 Q. Wang, X. Wu, L. Wang, Z. Chen and S. Wang, *Phys. Chem. Chem. Phys.*, 2014, **16**, 19351.
41 R. K. Mishra, S. K. Pandey and P. P. Sahay, *Mater. Res. Bull.*, 2013, **48**, 4196–4205.
42 C. Thomsen and S. Reich, *Phys. Rev. Lett.*, 2000, **85**, 5214–5217.
43 M. A. Pimenta, G. Dresselhaus, M. S. Dresselhaus, L. G. Cancado, A. Jorio and R. Saito, *Phys. Chem. Chem. Phys.*, 2007, **9**, 1276–1291.
44 E. Kayhan, R. M. Prasad, A. Gurlo, O. Yilmazoglu, J. Engstler, E. Ionescu, S. Yoon, A. Weidenkaff and J. J. Schneider, *Chem. – Eur. J.*, 2012, **18**, 14996–15003.
45 A. C. Ferrari, J. C. Meyer, V. Scardaci, C. Casiraghi, M. Lazzeri, F. Mauri, S. Piscanec, D. Jiang, K. S. Novoselov, S. Roth and A. K. Geim, *Phys. Rev. Lett.*, 2006, **97**, 187401.
46 P. K. Manoj, B. Joseph, V. K. Vaidyan and D. S. D. Amma, *Ceram. Int.*, 2007, **33**, 273–278.
47 M. E. White, O. Bierwagen, M. Y. Tsai and J. S. Speck, *Appl. Phys. Express.*, 2010, **3**, 51101–51103.
48 P. Offermans, H. D. Tong, C. J. M. van Rijn, P. Merken, S. H. Brongersma and M. Crego-Calama, *Appl. Phys. Lett.*, 2009, **94**, 223110.
49 M. Siemons and U. Simon, *Sens. Actuators, B*, 2007, **126**, 595–603.